Parametric Investigation of Laser-Driven Microrobot Maneuvrability on Dry Substrates

Sri Sukanta Chowdhury, Member, IEEE, Zhong Yang, Student Member, IEEE, Andriy Sherehiy, Ruoshi Zhang, Student Member, IEEE, Dan O. Popa, Senior Member, IEEE

Danming Wei, Student Member, IEEE, Dan O. Popa, Senior Member, IEEE

Abstract— ChevBot is a novel microrobot for operation in dry environments driven by focused energy from a Nd:YAG laser. The microrobot operates using stick-slip locomotion by converting opto-thermal energy from the focused laser source into mechanical energy using "chevron-style" actuators. ChevBot's body components are fabricated using Micro-Electro-Mechanical-System (MEMS) technology and completed using a microassembly process. In this paper, we investigate the effect of laser parameters such as pulse frequency, beam intensity and position to the maneuverability of the robot on planar substrates. The average microrobot forward speed could be varied between 1-134 µm/s by sweeping the laser pulse frequency from 900-1500 Hz. Experiments also suggest that the average speed of the ChevBot can also be controlled by varying the number of pulses and laser drive current. Furthermore, the ChevBot could be steered in both the clockwise and counterclockwise directions by positioning the laser spot in various locations on the ChevBot's microactuator.

Keywords— Microrobot, Microassembly, Microfactory, Control, Steering.

I. INTRODUCTION

Microrobots have potential to be used in a nano and bio applications due to their small size, weight, and reduced power consumption. Recently, a lot of research has been conducted toward achieving motion control of autonomous robots at the micro and nano scales by utilizing thermal, electrostatic, magnetic, piezoelectric, ultrasonic and laser energy as the actuating and powering source [1]. Among all these actuation techniques, electro-magnetic actuation was explored the most, where it is employed not only to drive the robots but also to accomplish open or closed-loop control of their motion [2-7]. Various phenomena related to electric and magnetic field interaction with the robot material were explored in order to accomplish controlled steering, for instance dielectrophoretic effect was used in order to realize controllable assembly of microrobots which can be steered by variable magnetic field [8].

Actuating a microrobot by a coherent light source i.e. a laser remotely is somewhat less popular most probably due to its directional nature. Furthermore, tracking is even more difficult because of the small field of view of a laser illumination. For example, James et al. [9] used a laser light as a source to indirectly deliver the energy to power a flying microrobot via solar cells. In addition, laser was successfully utilized both as power and control source for microscopic objects in liquid environments [19]. Others demonstrated "bubble microrobots" enabling open-loop manipulation tasks with different materials, targets, and parameters [10]. Further studies led to the development of the bubble microrobot systems with closed-loop control for the simpler tasks [11], and more recently for 3D manipulation and microassembly of 3D constructs [12]. Another extensively studied example of laser actuation of the microscopic objects is optical tweezing and trapping [13]. However, this method has been tried on a dry surface only by a very small number of researchers [20].

Recently, we introduced the ChevBot, a new class of light-driven microrobots that operates in dry surface more suitable for future microfactories. The ChevBot is fabricated with MEMS techniques and microassembly, which has an overall dimension of 300 μ m \times 500 μ m \times 40 μ m. In our work [14-17] we described opto-thermal-dynamical models of ChevBot operation based on the stick-and-slip motion along straight trajectories. Experimental validation of these models was performed with microrobots of different designs [15,16]. The ChevBot locomotion is realized with the help of chevron thermal actuators that connect the two ends of its body frame. Incident laser irradiation converts pulsed laser energy to mechanical motion due to temperature induced thermal expansion. Since the "feet" and the "dimple" are in contact with the substrate at different angle, this interaction generates a differential frictional force resulting in a stick and slip motion. In [16], we experimentally confirmed that laser driven ChevBot can follow approximately straight trajectories where the speed of the robot can be controlled by tuning laser parameters such as frequency and intensity. The simulation models of the ChevBot also predicted possible steering capabilities of this robot.

In this paper we designed and conducted experiments to measure the effect of laser parameters on the maneuverability of the ChevBot, expressed as forward velocity, and steering angle. Based on our past findings from models described in regarding directional motion maneuverability and controllability, a series of experiments were designed and conducted to realize repeatable controlled steering of the ChevBot. Results suggest that the ChevBot can be steered by large angles in the range of 8-40 degree by focusing the laser beam to different parts of the microrobot's thermal actuator, and that its speed can be controlled between 1-134 µm/s by varying the laser pulse frequency. Speed was also controlled between 15-119 μm/s by changing the number of pulses and the laser power. Furthermore, we demonstrate frequency differentiation between microrobot samples prototyped by microassembly from identical MEMS components. In the future, this behavior can be exploited to individually control multiple ChevBots operating in the same dry environment.

This paper is organized as follows: Section II represents details of ChevBot design and actuation mechanism; Section III describes cleanroom fabrication, microassembly and laser beam delivery set up; Section IV illustrates experimental results with two identical ChevBot samples; And finally, Section VI summarize the core findings along with a discussion of future work.

II. CHEVBOT: A MEMS MICROROBOT

ChevBot is a MEMS microrobot assembled from two main components called the body and the dimple, both

This work was supported by National Science Foundation Grant #CMMI 1734383

^{*}Authors are with the Louisville Automation and Robotics Research Institute (LARRI), University of Louisville, Louisville KY 40292. Email {firstname.lastname@louisville.edu}

fabricated in a cleanroom using Silicon. Silicon is chosen because of its excellent heat transfer properties as microactuators are actuated by opto-thermo-mechanical conversion. The body contains two feet extruding from the frame with an angle of 135° that supports the robot on a dry substrate, usually a polished silicon wafer or glass slide. The main actuators of the ChevBot are some chevron structures anchored with the body through a shuttle. The specific ChevBot studied in this paper has a total of 6 pairs of chevron beams, each has a dimension of $5\mu m \times 200\mu m \times 20\mu m$. These beams are at an angle of 87° with the frame of the ChevBot. The ChevBot measures $734~\mu m$ in length and $427\mu m$ in width and $40~\mu m$ in height at dimple position as shown in Figure 1 and detailed in [15].

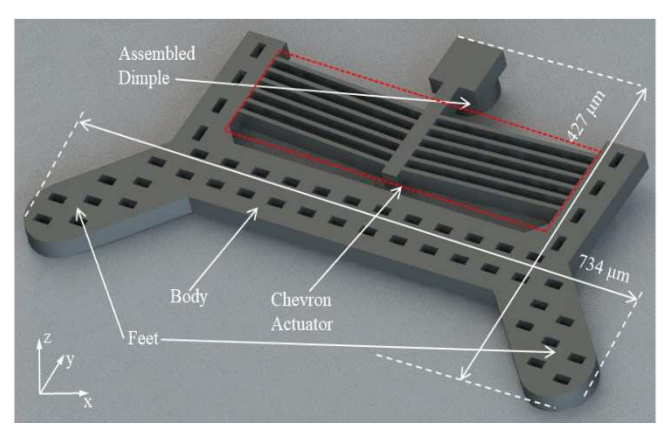


Fig. 1. An assembled ChevBot showing different parts along with its dimensions.

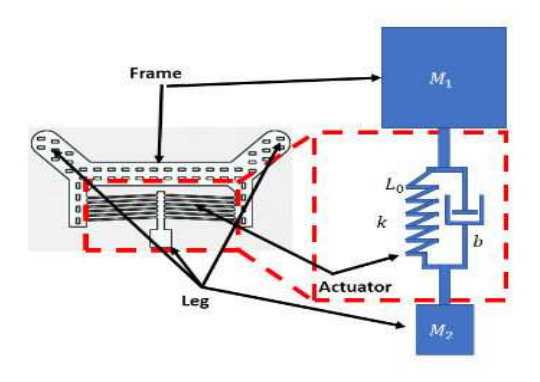


Fig. 2. Mass-spring-damper-mass model of ChevBot. M₁ is the mass of the ChevBot body, k is the effective spring constant of the chevron beams, b is the amount of damping due to viscous drag from air and substrate and M₂ is the mass of the dimple

This microrobot can be modeled as a lumped-element mass-spring-damper-mass system as shown in Figure 2. Because the mass of the dimple is negligible compare to the overall mass of the ChevBot, it is ignored in this model. Such a mechanical system can be mathematically expressed as a second order differential equation:

$$M_1 \frac{d^2x}{dt^2} + b \frac{dx}{dt} + kx = F \tag{1}$$

where F is the net force acting on the ChevBot, M_I is the mass of the robot body, b is the damping coefficient of viscous drag on the ChevBot resulting from the presence of surrounding air and k is the effective spring constant of the Chevon beams. In a situation when there is no external

excitation driving the ChevBot, it still oscillates with a very small amplitude because of the internal thermal energy. Power spectral density $S_x(f)$ of the motion of such self-excited structure is given by the Lorentzian [17]:

$$S_{x}(f) = \frac{\frac{\bar{x}^{2}}{\pi Q f_{0}}}{\left(1 - \left(\frac{f}{f_{0}}\right)^{2}\right)^{2} + \left(\frac{f}{Q f_{0}}\right)^{2}} \tag{2}$$
the expected value of amplitude of vibration Q

where \bar{x} is the expected value of amplitude of vibration, Q is the quality factor and f_0 is the resonance frequency, given by

$$f_0 = \frac{1}{2\pi} \sqrt{k/M_1} \ . \tag{3}$$

For a fixed ChevBot, the resonance frequency increases and decreases as the stiffness of the structure changes accordingly. Stiffness on the other hand depends on the boundary condition such as the roughness of the media surface the ChevBot is placed on. Stiffness also depends on the angle the ChevBot makes with the surface as well as the exact position of the dimple on the robot. Quality factor, that defines the degree of the resonance is expressed as

$$Q = 2\pi m f_0/b \tag{4}$$

It is evident from eq. (4) that quality factor is inversely proportional to the damping coefficient. This is why amplitudes of small vibrations are often measured in vacuum where the drag force is negligible. The governing eqs.1-4 are equally valid if the ChevBot is driven by an external excitation e.g. driven by a pulsed laser. For such externally excited structures, which is true for our case, the amplitude of the vibration in eq. (2) would increase significantly, which explains the stick and slip mechanism we explained in our earlier reports [14-15].

III. FABRICATION, MICROASSEMBLY AND LASER BEAM DELIVERY

Designing and assembling a ChevBot is a multistep process begins with a CAD design which is ultimately used to write a photolithography mask. Detail of these steps are in subsequent sections.

A. Fabrication of ChevBot body and Dimple

The fabrication process begins with a 4-inch SOI wafer with orientation of <100> consist of a 20 μm device layer and a 2 μm buried oxide layer. After cleaning, a layer of SPR220-3.0 photoresist is coated on the surface of the silicon wafer. The resist layer is thinned down to $3\mu m$ using a spinner rotated at a required profile. Then the photoresist is patterned with a Suss Mask Aligner MA6/MA8 and developed subsequently with a ramp up and down temperature profile to avoid cracking of the photoresist layer. Once the photoresist is properly developed, a deep reactive ion etching (DRIE) is performed by SPTS DRIE to create the ChevBot feature on the wafer. The wafer is then diced into 1 by 1 cm dies. As a final cleanroom step, each structure in a die is released by a dry etch process, through uEtch® HF vapor MEMS Etch Release System.

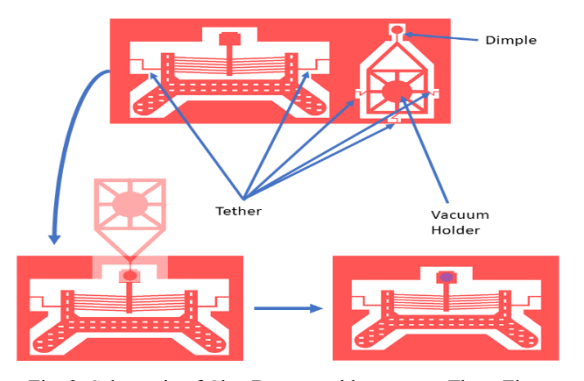


Fig. 3. Schematic of ChevBot assembly process. Three Figures represent body and dimple before assembly, after assembly and after untethering the dimple handle.

Dimples of two different shapes (circular and square) and 3 different sizes (50,60,70 um) are exposed and patterned on the same 4-inch wafer. But the releasing process is carried out using a dry etch technique to avoid the irregular etching and sticking problem that arise because of larger area of these patterns. Dry etch is performed using a VHF process for 8 hours.

B. Assembly Process

The ChevBot assembly is a 4-step process performed using three separate instruments. In the first step of the assembly, a micro probe station, as shown in Figure 5, is used to untether the dimples from the dies. First, the die is placed on the stage and aligned with the field of view of the microscope. Two micro probes are brought on top of the tethered dimple and untethered the dimple along with its handle using them.

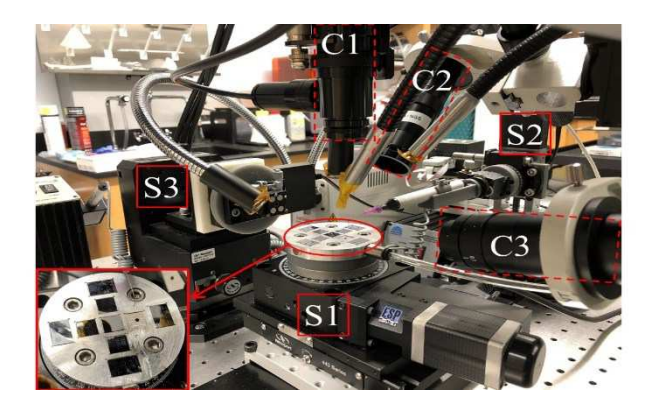


Fig. 4. NeXus microassembly station. $S_1\text{-}S_3$ represents stacked stages and $C_1\text{-}C_3$ shows the cameras.

Second step in the assembly is performed at NeXus microassembly station as shown in Figure 4. This microassembly station consists of 3 manipulators (stacked stages) and 3 cameras along with 3 fiber optic light pipes for illumination. Camera C1 is vertically aligned with the bottom stage S1 which gives a direct top view of the underlying dice. Camera C2 and C3 are placed at an angle of approximately 45 and 30 degree from front and right side of the user respectively. Motorized stage S1 consists of two identical linear stages and a rotational stage cascaded vertically. A sample chuck made of aluminum is placed on top of the

topmost stage that hold the sample dies. The chuck has five 1 cm by 1cm die holders secured by an integrated vacuum seal connected to the main vacuum line in the lab. This stage along with the sample chunk is used to move the dies containing the ChevBots and dimples in X, Y and θ direction to align them with the cameras as well as a vacuum tip connected to S2 manipulator. S2 manipulator is consists of a manual Z stage, used for coarse height adjustment, three linear stages and one rotational stage all stacked together as shown in Figure 4. The rotational stage is mounted on the Z stage with a custom built, 3D printed fixture along with an adapter and a vacuum tip end-effector in a way so that it faces toward the user. The vacuum tip is bend at 90 degree downward, vertically aligned with the ChevBots and dimples.

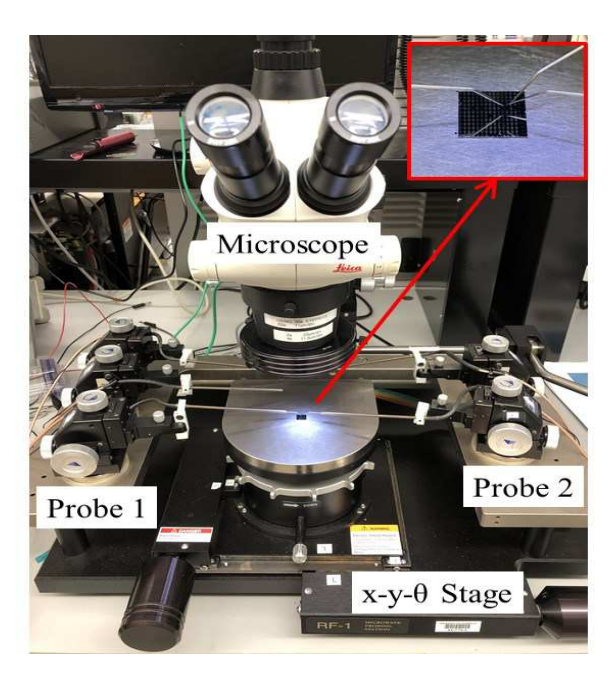


Fig. 5. Probe station with integrated travelling microscope and stages.

For assembling the ChevBots, the vacuum tip is aligned vertically on top of the dimple handle pad and brought closer using the manipulator S2. The vacuum tip is brought even closer gradually with very slow speed (0.1-0.01 mm/step) until the dimple is picked up by the vacuum tip. The vacuum tip, along with the picked-up dimple is then brought on top of this drop of UV adhesive (BONDIC L4G 3V5, Aurora, ON, Canada) and lowered down slowly until bottom surface of the dimple touches the meniscus of the drop. The vacuum tip and the attached dimple are then brought on top of the ChevBot body located in another die. Manipulator S1 is now used to align the dimple with the assembly pad of the ChevBot and lowered down gradually until the glue attached to the lower surface of the dimple touches the assembly pad of the ChevBot. The vacuum is then turned off and the tip is pulled off the sample die.

The third step in the assembly process is the curing of the UV glue. A NOVASCAN PSD-UV benchtop curing machine is used for this purpose. The die containing the assembled ChevBots are placed in the UV chamber on a sample stand (two inches in height) and positioned at the UV chamber, keeping the sample dice 1.5 inches below the lamp. The

temperature is set at 32° C and the samples are cured for 30 minutes. The samples are left overnight in the chamber and another curing cycle is performed using the same configuration after 12 hours of initial curing. This two-step curing process is developed after certain trial and error process.

The fourth and the final step in the assembly process is untethering the assembled robots from the die. Microprobe station used for untethering the dimple is used again at this step. First, the body of the ChevBot is secured by placing a probe touching the frame and then the handle of the dimple is pushed by another probe to break. Then, rest of the tethers of the ChevBot is broken with the same probe. After that, a micromanipulator, basically a sharp needle, is gently touched on the frame of the untethered ChevBot. Sometimes but not always, the ChevBot is stacked to the needle tip due to electrostatic force. At that point, the micromanipulator along with the attached ChevBot is taken away from the dice and placed on a clean 2 cm by 2 cm silicon wafer.

C. Laser beam delivery

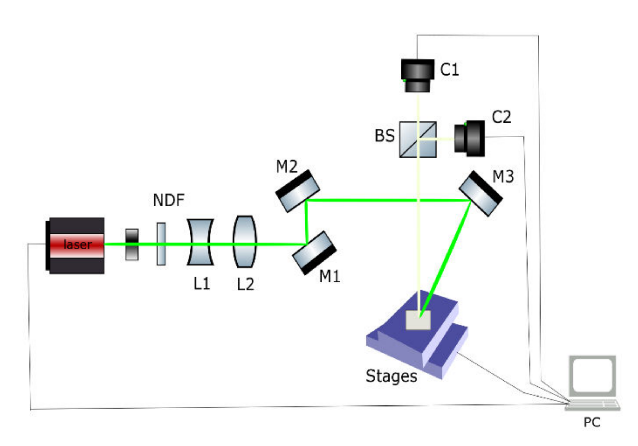


Fig. 6. Laser beam delivery system along with smart camera for tracking and stages for trajectory acquisition.

The main power source of the ChevBot is a Nd:YAG pulse laser from Spectra-Physics operates at 532 nm wavelength. Frequency of the pulses can be adjusted between 0.5-60 KHz, with a pulse width ranging from 10-40 ns, outputting optical power (time averaged) as high as 2.0 W. A schematic of the optical set-up is shown in Figure 6. The laser output port is connected to a black metallic cylinder with a Uniblitz optical shutter at the other end of the cylinder. This is a precautionary measurement to protect the users while they change the ChevBot. There is a variable neutral density filter wheel followed by the shutter. The filter strength is adjustable between 0.01-5 OD and used to real-time monitoring of the laser spot position on the ChevBot while an adjustment is needed. A bi-concave lens L1 is used to expand the beam before it reaches the bi-convex lens L2. Relative distance between L1 and L2 is varied to reach the desired spot size at the sample location. Three mirrors are used to guide the beam to the sample. Mirror M1 deflect the beam path at a 90-degree angle, M2 is used for coarse and M3 is used for fine adjustment of the beam position. A National Instrument smart camera (ISC-1772C) is connected to a tube lens through a beam splitter, used for tracking the ChevBots.

Another camera (Pixelink PL-D734) is connected to the other face of the beam-splitter, used for visualization and recording the ChevBot motion. The sample chuck is placed on a stack of 4 linear stages. All the stages are from Newport 423 and 443 series, of which, two of them are controlled by TRA25CC linear actuator and the rest two are controlled manually.

IV. EXPERIMENTAL RESULTS

A. Finding the resonance

Two ChevBots are used in these experiments to validate the role of resonance frequency in their locomotion. Theoretically all the ChevBot would have the same resonance frequency if placed on an identical surface as their dimensions are precisely controlled during the cleanroom fabrication. In reality, we observed some differences which we believe are due to the variations in the assembly process. These variations come from the difference in the amount of UV glue placed on each ChevBot as well as the location of the dimple on the pad. Figure 7 illustrates the findings of the experiments conducted to determine the resonance frequencies of two sample of ChevBots

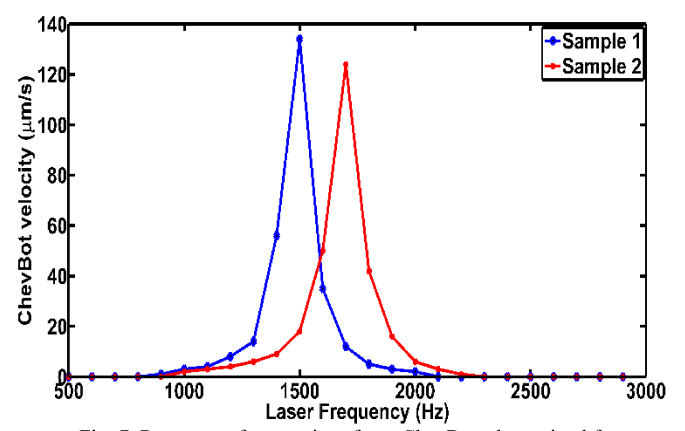


Fig. 7. Resonance frequencies of two ChevBots determined from frequency sweep experiments.

The ChevBots are illuminated with laser beam aligned with their center. Laser is operated in burst mode with 50 pulses per burst and a delay of 300 ms between individual burst. The driving current is kept constant at 4.8 A along with the delay and number of pulses throughout the experiments. The frequency (pulse repetition frequency) of the laser is varied between 500-3000 Hz with a 100 Hz increment. Each time the laser is set at a frequency followed by opening of illumination by optical shutter for approximately 1 second. Simultaneous capturing of video of ChevBot movement is conducted. The ChevBot is brought back to the field of view of the laser manually and the frequency is increased to the next step. The whole process is repeated throughout the frequency span. Average speed of the ChevBot is determined by comparing the initial and final position and corresponding time. The resonance frequency of the first sample is found to be at 1500 Hz compare to the second sample at 1700 Hz. These values are similar to our previous reports using the same family of the ChevBots. None of these MEMS structures were responsive below 800 Hz and above 2300 Hz.

Sample 1 starts movement at 900 Hz with a small average speed of 1 μ m/s and reaches its maximum value of 134 μ m/s at 1500 Hz and then falls sharply to 2 μ m/s at 2000 Hz. Sample 2 shows a similar trend except that its maximum average speed is observed at 1700 Hz. Note that the average speed reported here is larger than our previous reports. These increases are because of using a smaller laser spot and reduction in amount of UV glue during assembly process. The difference in resonance frequency is 200 Hz, which is more than 10%, despite the precise fabrication and assembly process. This is due to the slight variation in the amount of glue during the assembly, which may be avoided by eliminating the assembly process altogether and fabricating the whole microrobot in cleanroom.

B. Steering by Off-axis illumination

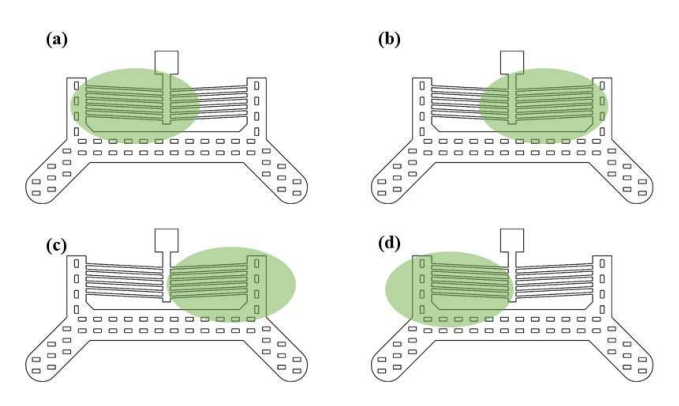


Fig. 8. Laser spot positioning on the ChevBot for steering by off-axis illumination.

This specific design of ChevBot reported here only moves in a forward direction about 90% of the time if the laser beam is illuminated at its center. There has been some steering effect observed but the repeatability was rather small. Steering is crucial for controlling the trajectory of these tiny structures. As an attempt to achieve the steering, illumination at different parts are conducted. Laser spot positioning for this experiment is illustrated in Figure 8.a-d. Figure 9.a-d. shows corresponding initial and final positions of Sample 1, overlapped in a single image, before and after the laser beam incident on the ChevBot. The non-spherical shape of the laser spot is due to the inclined illumination to keep the line of sight of the cameras clear of obstacles as shown in Figure 6.Laser drive current in these measurements is set at 4.5 A which corresponds to a power output of 270 mW and the frequency is set at 1500 Hz with a total illumination time of 1 second. In fig.9(a), the laser beam covers the two third of the ChevBot from the left while leaving rest of the chevron beams in right side unilluminated. The ChevBot rotates clockwise by 8 degree and its center displaced by 77 µm. In fig.9(b), the laser beam covers the two third of the ChevBot from the right side. For this configuration, the ChevBot rotates counterclockwise by 10 degree with 242 μm of displacement. Fig.9(c) shows the extreme case of the laser beam positioning where only the right half of the ChevBot is illuminated which resulted in a 40degree clockwise rotation with a large 341 µm displacement. In the final sub image of 9(d), the laser beam is positioned to cover only the left half of the ChevBot. This configuration again produced a clockwise rotation of 16 degree and 127 µm of displacement. The tendency of clockwise rotation of this

ChevBot is probably due to the misalignment of the dimple during assembly process.

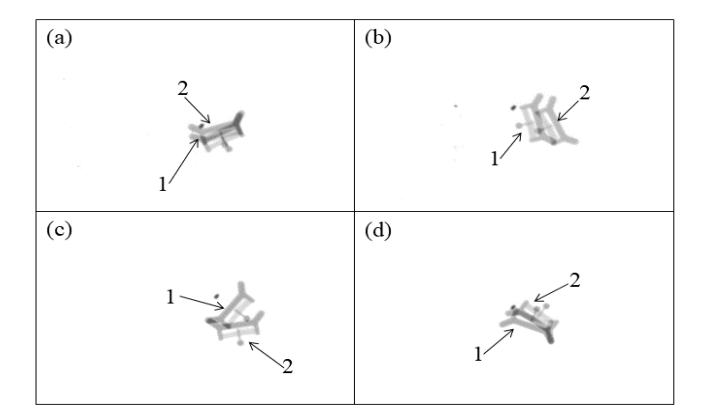


Fig. 9. Steering by off-axis illumination. (1) represents the initial robot position, and (2) represents the final position after illumination for a fixed 1s duration.

C. Average speed vs number of pulses & power

The pulse laser used in this study has some user features that can be controlled programmatically. One of the goals of this study is to develop a control algorithm to modify the laser parameters so that the ChevBot moves in a predefined trajectory. This experiment is conducted to better understand the correlation of the number of pulses on the average speed of the ChevBots. While the number of pulses delivered in a burst does not change the average power to a significant amount it does however have an impact on the acceleration (which means average speed as well).

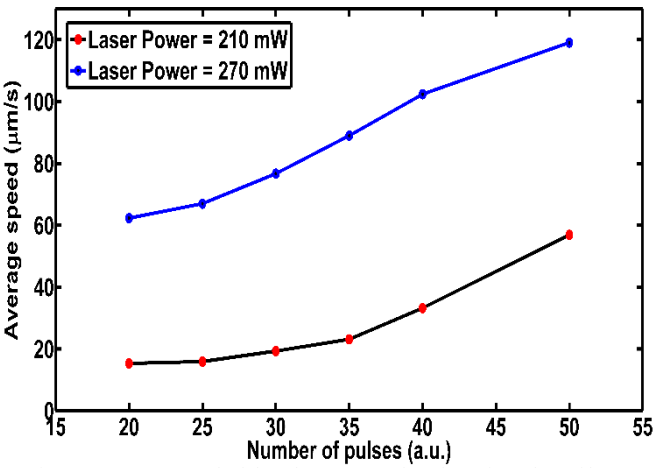


Fig. 10. Average speed of the ChevBot as a function of number of laser pulses and power.

Only sample 1 is used during this experiment where the number of pulses delivered to the ChovBot is varied between 20-50 for two different power levels of 210 nad 270 mW. As seen from Figure 10, average speed of the ChevBot increases as the number of pulses increases. For 210 mW power, the lowest average speed is 15.3 $\mu m/s$ that goes up to 56.9 $\mu m/s$ as the pulse number increases to 50. This trend is equally valid for a higher power of 270 mW as depicted by the blue curve in Figure 10.

V. DISCUSSION AND CONCLUSION

Controlling the movement of a microrobot is a scientifically challenging problem and using a pulsed laser to actuate structures on dry surfaces is inherently more difficult due to the directional nature of the laser energy and variations in surface conditions. In this paper, the microrobot's movements were observed carefully in order to understand the underlying mechanism that drives or impedes their motion. The ChevBot's design along with control parameters such as laser power, number of pulses, laser beam positioning on the microrobot as well as the roughness of the media contribute to the microrobot's overall performance. In this paper, we have shown that the resonance frequency dominates the speed of ChevBots. This work represents a significant validation of concept that will allow microrobot researchers to design and test the performance of Chevron microrobots driven by laser and will guide them towards achievement of autonomy at micro scales. In this paper, we demonstrated that changing the laser beam position is a viable option for steering the chevron-based microstructures that are difficult due to their inherent design characteristics. This observation could be utilized by using a MEMS micromirror to rapidly scan the laser beam on a ChevBot. This type of micromirrors are used successfully in augmented reality headsets to produce custom illumination pattern in order to form images. The third important laser parameter is the number of pulses delivered to the ChevBot at a time. This mode of laser operation is known as burst mode and is found to be quite helpful to give the structures some time to cool down. The number of pulses at a given power has a positive correlation with the average speed of the ChevBots.

In summary, resonance frequency which is the result of a specific design, along with the laser beam positioning and number of pulses can be used to modify and guide the locomotion of chevron-based structures. Average speed of the Chevbots was varied from 1-134 µm/s by changing the laser frequency between 900-1500 Hz. Spot illumination of fixed duration turns them between 8-40 degrees both in clockwise and counterclockwise directions. Average speed was also controlled between 15-119 µm/s by varying the number of pulses and the laser power. These parameters are by no means the only contributing factors that determines the trajectory of a ChevBot but the most important ones besides the surface roughness of the media. Our next step in this research will be exploration of the surface roughness of different dry media and implementation of a trajectory controller to achieve micro scale autonomy.

ACKNOWLEDGMENT

We wish to thank the Micro Nano Technology Center (MNTC) staff at the University of Louisville, for their help with cleanroom fabrication. Sincere thanks to Mariah B Hall for assembling the ChevBots during this study

REFERENCES

[1] E. Y. Erdem, Y.-M. Chen, M. Mohebbi, J. W. Suh, G. T. A. Kovacs,
 R. B. Darling and K. F. Böhringer, "Thermally Actuated Omnidirectional Walking Microrobot," Journal of

- Microelectromechanical Systems, vol. 19, no. 3, pp. 433-442, June 2010
- [2] M. P. Kummer, J. J. Abbott, B. E. Kratochvil, R. Borer, A. Sengul and B. J. Nelson, "OctoMag: An Electromagnetic System for 5-DOF Wireless Micromanipulation," IEEE Transactions on Robotics, vol. 26, no. 6, pp. 1006-1017, 2010.
- [3] E. Diller, S. Floyd, C. Pawashe and M. Sitti, "Control of Multiple Heterogeneous Magnetic Microrobots in Two Dimensions on Nonspecialized Surfaces," IEEE Transactions on Robotics, vol. 28, no. 1, pp. 172-182, 2012.
- [4] S. Song, S. Song and M. Q. -. Meng, "Electromagnetic actuation system using stationary six-pair coils for three-dimensional wireless locomotive microrobot," 2017 IEEE International Conference on Information and Automation (ICIA), Macau, 2017, pp. 305-310.
- [5] P. Ryan and E. Diller, "Magnetic Actuation for Full Dexterity Microrobotic Control Using Rotating Permanent Magnets," IEEE Transactions on Robotics, vol. 33, no. 6, pp. 1398-1409, 2017.
- [6] E. E. Hunter, E. B. Steager, A. Hsu, A. Wong-Foy, R. Pelrine and V. Kumar, "Nanoliter Fluid Handling for Microbiology Via Levitated Magnetic Microrobots," IEEE Robotics and Automation Letters, vol. 4, no. 2, pp. 997-1004, 2019.
- [7] J. Giltinan and M. Sitti, "Simultaneous Six-Degree-of-Freedom Control of a Single-Body Magnetic Microrobot," IEEE Robotics and Automation Letters, vol. 4, no. 2, pp. 508-514, 2019.
- [8] Y. Alapan, B. Yigit, O. Beker, A. F. Demirörs and M. Sitti, "Shape-encoded dynamic assembly of mobile micromachines", Nature Materials, vol. 18, pp. 1244–1251, 2019
- [9] J. James, V. Iyer, Y. Chukewad, S. Gollakota and S. B. Fuller, "Liftoff of a 190 mg Laser-Powered Aerial Vehicle: The Lightest Wireless Robot to Fly," in 2018 IEEE International Conference on Robotics and Automation (ICRA), Brisbane, Australia, May 21-25, 2018.
- [10] K. S. Ishii, W. Hu and A. T. Ohta, "Cooperative micromanipulation using optically controlled bubble microrobots," in IEEE International Conference on Robotics and Automation, Saint Paul, MN, USA, 2012.
- [11] N. Takahashi, Z. Wang, M. A. Rahman, J. Cheng and A. T. Ohta, "Automated micro-object caging using bubble microrobots," in 2016 IEEE 11th Annual International Conference on Nano/Micro Engineered and Molecular Systems (NEMS), Sendai, Japan, April 2016.
- [12] L. Dai, Z. Ge, N. Jiao, and L. Liu, "2D to 3D Manipulation and Assembly of Microstructures Using Optothermally Generated Surface Bubble Microrobots", Small, vol. 15, 1902815, 2019
- [13] H. Chen, C. Wang, X. Li and D. Sun, "Transportation of Multiple Biological Cells Through Saturation-Controlled Optical Tweezers in Crowded Microenvironments," IEEE/ASME Transactions on Mechatronics, vol. 21, no. 2, pp. 888-899, 2016.
- [14] M. R. Pac and D. O. Popa, "3-DOF Untethered Microrobot Powered by a Single Laser Beam Based on Differential Thermal Dynamics," in 2011 IEEE International Conference on Robotics and Automation, Shanghai, China, 9-13 May 2011.
- [15] R. Zhang, A. Sherehiy, Z. Yang, D. Wei, C. K. Harnett and D. O. Popa, "ChevBot – An Untethered Microrobot Powered by Laser for Microfactory Applications," in 2019 International Conference on Robotics and Automation, Montreal, Canada, 2019.
- [16] R. Zhang, A. Sherehiy, D. Wei, Z. Yang, M. Nasser Saadatzi, D. O. Popa, "Tracking Experiments with ChevBot: A Laser-Actuated Stick-Slip Microrobot", in *International Conference on Manipulation*, Automation and Robotics at Small Scales (MARSS), Helsinki, Finland, 2019.
- [17] Z. Yang, M. N. Saadatzi, R. Zhang, A. Sherehiy, D. Wei, K. C. Harnett and D. O. Popa, "Multiphysics Dynamic Model Validation Methodology for Laser-Driven Microrobots," in 2019 IEEE 15th International Conference on Automation Science and Engineering, Vancouver, Canada 2019.
- [18] S. S. Chowdhury, A. Sherehiy, C. Jarro and R. W. Cohn, "Optical Measurement of Thermal Vibration Spectra to Determine Young's Modulus of Glass Microfibers" in 2018 IEEE 13th Nanotechnology Materials and Devices Conference (NMDC), Portland, Oregon, USA 2018
- [19] H. Zeng, P. Wasylczyk, D. S. Wiersma, A. Priimagi, "Light Robots: Bridging the Gap between Microrobotics and Photomechanics in Soft Materials," Advanced Materials, vol. 30, issue 24, article 1703554, June 13, 2018.
- [20] Uchida, E., Azumi, R. & Norikane, Y. "Light-induced crawling of crystals on a glass surface." Nat Commun 6, 7310 (2015).